

Suppressing Coherent Synchrotron Radiation Effects in Chicane Bunch Compressors

Fancong Zeng,¹ Yi Jiao,^{1,*} Weihang Liu,² and Cheng-Ying Tsai³

¹*Key Laboratory of Particle Acceleration Physics and Technology,
Institute of High Energy Physics, Chinese Academy of Sciences,
and University of Chinese Academy of Sciences, Beijing 100049, China*

²*China Spallation Neutron Source, Institute of High Energy Physics,
Chinese Academy of Sciences, Dongguan 523803, China*

³*School of Electrical and Electronic Engineering, Huazhong University of Science and Technology, Wuhan 430074, China*

(Dated: March 19, 2024)

The most significant advances in the accelerator-based light sources (i.e., x-ray free electron lasers) are driven by the production of the high final peak current in the last several decades. As a prerequisite to attain the proposed high brightness, the symmetric C-chicane bunch compressor is typically exploited due to its simplicity, efficiency, and natural dispersion-free feature at all orders. However, during bunch compression for a high peak current requirement, a main contributing factor to the transverse emittance degradation is the emission of the coherent synchrotron radiation (CSR). Suppressing this effect is necessary to preserve the beam phase-space quality. To this end, this paper presents an analysis of one-dimensional CSR point-kick and derives the cancellation conditions in terms of compression factor. The CSR cancellation conditions indicate an asymmetric geometric design. We demonstrate concrete schemes for asymmetric C- and S-chicanes, and verify the CSR cancellation conditions using integration methods and ELEGANT simulations. Furthermore, the proposed asymmetric C- and S-chicanes can drastically suppress the emittance growth compared with the symmetric ones with identical bunch compression goals.

I. INTRODUCTION

The advent of accelerators and accelerator-based light sources has revolutionised the development of science, industry, medicine, and materials research. In contemporary accelerators, electron bunch compressors play a pivotal role, with wide applications in linear colliders [1], linacs [2], beam-driven plasma-wakefield accelerators [3, 4], and significant application in free electron lasers (FELs) [5–9]. Combined with the position-energy correlation provided by the RF cavity, the following dispersive element helps to convert the energy difference into a difference in the time of flight of the particles. This causes the particles at the head and tail to become closer, enabling beam compression.

Currently, the symmetric C-chicanes with four bending magnets are the most commonly used bunch compressors in accelerator systems, because such chicanes are simple, effective and of course, dispersion-free at all orders [10]. However, with the high compression factor and ~kiloampere level peak current required for FELs, the expected FEL performance is hard to preserve due to the coherent synchrotron radiation (CSR) effect [11–15]. When an electron bunch travels in a curved path, it is possible for the coherent radiation emitted by the trailing particles can interact with the leading particles within the dipole, spoiling the transverse beam quality. This effect is particularly noticeable in cases of high bunch current and short bunch length. As a consequence of the CSR effect, the emission of the CSR leads to transverse emittance growth, which is more obvious in the final two dipoles of the chicane, where the bunch becomes shorter [5]. Not only are there transverse effects, but also the short-range wake driven microbunching instability (MBI) resulting from density-energy

modulations, in the longitudinal plane, can also be a potentially detrimental phenomenon [15–23]. To alleviate this difficulty, various efforts have been stimulated, including analytical, numerical, and experimental studies to suppress the CSR effect in the past decade [24–42].

To suppress the CSR-induced emittance growth, one mitigation approach exploited the correlation between the CSR and the longitudinal distribution of the beam, using longitudinal shaping [25, 26] or using a longitudinal transverse emittance exchanger [27, 28], or other complex means. Experimentally, Ref. [29] observed that CSR wakes in a bending magnet could be minimised by using shielding plates. On the other hand, the approach of suppressing CSR by manipulating beam optics has sparked continuing research interest. The optical balance method was first proposed by D. Douglas [30], and further developed by the Courant-Snyder formalism analysis [34]. Moreover, emittance dilution can be compensated for in a single achromatic cell by matching the beam envelope to the CSR-induced dispersion [31]. An investigation proved that the beam envelope matching and Courant-Snyder analysis are equivalent to each other, and indicated that the complicated CSR in dipole can be evaluated with a (x, x') 2D point-kick analysis [32]. The optical balance method and further study have been successfully applied to many scenarios, e.g., spreader, double-bend achromats (DBAs), triple-bend achromats (TBAs) [33–35], and even compression systems, e.g., DBA-based compressors [36].

The attempts of cancelling the CSR-driven emittance excitation in chicanes have been a long-standing question. Classified from the four-bend chicane geometries, there are four chicane designs available, including symmetric (asymmetric) C- and S-chicanes. Additionally, if the number of dipoles is not limited, five- and six-bend chicanes are also proposed or applied [24, 42–44]. A symmetric chicane (including symmetric four- and six-bend chicanes) is easy to design for a

* jiaoyi@ihep.ac.cn

fixed design goal, whereas almost all asymmetric chicanes are given by scanning chicane parameters [24, 42]. For example, one study [42] demonstrated a chicane with five dipoles of equal length and different bend angles, to suppress the CSR-induced emittance degradation. Compared with the symmetric C-chicane, the five-bend design achieves much better emittance suppression, suggesting the potential of increasing the degrees of freedom for a chicane to suppress the CSR effect. The parameter scanning method may be effective for a specific chicane design. Here we study the CSR-immuned chicanes on a consolidated basis of theoretical guidance, making our results easily transferable to arbitrary chicane design.

Inspired by the successful application of the point-kick model to a DBA-based compressor [36], this paper uses the same model to calculate the CSR effect for a chicane bunch compressor. However, due to the accumulation of the CSR effect at the chicane exit and the bunch length variation during compression, the theoretical design of a CSR-immune chicane is much more difficult. In this respect, the point-kick model [32] can greatly simplify the CSR effect and compression process. This allows us to derive analytical CSR cancellation conditions for the chicane bunch compressor with the aid of the point-kick model.

The purpose of this paper is to conduct a four-bend chicane, which consists of four dipoles separated by three drifts. It is assumed that the four bending angles and three drift lengths are free variables. Indeed, these variables are not completely free, as they must satisfy the achromatic condition, CSR cancellation conditions, and ensure that the beam returns to its horizontal trajectory (called ‘‘beam collinear condition’’).

For the sake of simplicity, we adopt four assumptions. We refer to the assumptions in the theoretical analysis in [36] for a review. First, we assume an electron bunch of Gaussian temporal distribution. Second, we assume a linear compression process during the electron bunch passing through the RF cavity and the chicane. Third, the analysis of the one-dimensional CSR physical model is restricted to the steady-state regime and in free space without beam pipe shielding, and for the moment excludes other effects such as transient CSR and space charge effects. Lastly, we ignore the influence of the conducting walls of the vacuum chamber. In this paper, we do not explore these assumptions any further and concentrate exclusively on the CSR effect in bunch compression.

This paper is organized as follows. With the CSR point-kick analysis, the conditions for suppressing the emittance growth due to CSR in a chicane can be obtained, as introduced in Sec. II. After satisfying the achromatic condition, CSR cancellation conditions, and beam collinear condition, we find that the chicane has an excessive number of degrees of freedom. To specify the design of the chicane, in Sec. III, we use two identical dipoles to mimic the structure of a symmetric C-chicane. The calculation result shows that a ‘‘negative drift’’ between the 2nd and 3rd dipoles is required. Then the question arises, whether there exists a chicane that can achieve the CSR cancellation with all positive drifts between the dipoles. To this end, we demonstrate that it is a S-chicane geometry, which has never been proved analytically (Sec. IV A). The specific asymmetric S-chicane design are introduced in Sec.

IV. In addition, both the integration method and ELEGANT particle tracking are used to verify our calculation results. We also compare the emittance growth of the symmetric C- and S-chicanes with that of the asymmetric ones, while maintaining identical bunch compression targets in Sec. V. Summary and discussion are presented in Sec. VI.

II. FORMALISM

A. chicane optics

First, an overview of the chicane linear optics is given. We consider a chicane consisting of four different dipoles separated by three adjustable drifts. The total transfer matrix of such chicane can be written as

$$M_{tot} = R_{B4}R_{d3}R_{B3}R_{d2}R_{B2}R_{d1}R_{B1}. \quad (1)$$

The 4×4 transfer matrix of a small-angle dipole R_{Bi} ($i = 1, 2, 3, 4$) in the horizontal and longitudinal planes (x, x', z, δ) can be expressed by

$$R_{Bi} = \begin{bmatrix} 1 & \rho_i\theta_i & 0 & \frac{\rho_i\theta_i^2}{2} \\ 0 & 1 & 0 & \theta_i \\ \theta_i & \frac{\rho_i\theta_i^2}{2} & 1 & \frac{\rho_i\theta_i^3}{6} \\ 0 & 0 & 0 & 1 \end{bmatrix}, \quad (2)$$

where ρ_i and θ_i are the beam bending radius and angle, respectively. And the transfer matrix of a half dipole can be obtained by replacing θ_i with $\theta_i/2$. We write the transfer matrix R_{di} of the drift as

$$R_{di} = \begin{bmatrix} 1 & L_{di} & 0 & 0 \\ 0 & 1 & 0 & 0 \\ 0 & 0 & 1 & 0 \\ 0 & 0 & 0 & 1 \end{bmatrix}, \quad (3)$$

where L_{di} ($i = 1, 2, 3$) is the drift length.

We aim to study the achromatic condition and the beam collinear condition uncovered by the chicane optics. With the total transfer matrix in Eq. (1), the achromatic condition $(M_{tot})_{16} = 0$, $(M_{tot})_{26} = 0$ and the first-order momentum compaction $R_{56}^{s_0 \rightarrow s_f} = (M_{tot})_{56}$ for the chicane can be calculated with

$$\begin{aligned} (M_{tot})_{16} &= L_{d1}\theta_1 + L_{d2}(\theta_1 + \theta_2) + L_{d3}(\theta_1 + \theta_2 + \theta_3) \\ &+ \frac{\theta_4}{2}L_{B4} + \frac{\theta_3}{2}(L_{B3} + 2L_{B4}) + \frac{\theta_2}{2}(L_{B2} + 2L_{B3} + 2L_{B4}) \\ &+ \frac{\theta_1}{2}(L_{B1} + 2L_{B2} + 2L_{B3} + 2L_{B4}) = 0, \\ (M_{tot})_{26} &= \theta_1 + \theta_2 + \theta_3 + \theta_4 = 0, \\ R_{56}^{s_0 \rightarrow s_f} &= L_{d1}\theta_1\theta_2 + L_{d3}\theta_3\theta_4 + \frac{L_{B1}}{6}\theta_1(3\theta_2 + \theta_1) \\ &+ \frac{L_{B2}}{6}\theta_2(3\theta_1 + \theta_2) + \frac{L_{B3}}{6}\theta_3(3\theta_4 + \theta_3) + \frac{L_{B4}}{6}\theta_4(3\theta_3 + \theta_4), \end{aligned} \quad (4)$$

where $L_{Bi} = \rho_i\theta_i$ is the dipole length, and the chicane entrance and exit are denoted by subscripts ‘‘ s_0 ’’ and ‘‘ s_f ’’ respectively.

The first two members of Eq. (4) have a double meaning. As a key feature of a lattice with only dipoles, the beam collinear condition (or called ‘‘geometric horizontal condition’’) that the horizontal trajectory of the beam is coaxial before and after passing through the chicane, coincides with the achromatic condition. For this reason, the beam collinear condition can be achieved naturally. For the length of bending magnet much shorter than the drift length, the dipole length L_{Bi} is typically neglected, which is appropriate for most chicane design scenarios. Thus Eq. (4) can lead to simpler expressions as

$$\begin{aligned} (M_{tot})_{16} &= L_{d1}\theta_1 + L_{d2}(\theta_1 + \theta_2) + L_{d3}(\theta_1 + \theta_2 + \theta_3) = 0, \\ (M_{tot})_{26} &= \theta_1 + \theta_2 + \theta_3 + \theta_4 = 0, \\ R_{56}^{s_0 \rightarrow s_f} &= L_{d1}\theta_1\theta_2 + L_{d3}\theta_3\theta_4. \end{aligned} \quad (5)$$

Dispersion cancellation is essential for chicane design to prevent dispersion-induced emittance growth caused by the momentum dispersive effect. In the following, we focus more on the CSR cancellation conditions for a chicane bunch compressor.

B. Application of CSR point-kick model to chicane

We apply a CSR point-kick model to analyze the steady-state CSR effect. As introduced in Ref. [30], the CSR effect induced in a dipole can be formulated equivalently with a point-kick at the center of the dipole. The idea is illustrated in Fig. 1. Such point-kick leads to a horizontal coordinate deviation in (x, x') plane and an energy deviation δ , which have the form of [32]

$$X_k = \begin{bmatrix} x_k \\ x'_k \end{bmatrix} = \begin{bmatrix} \rho^{4/3} k [\theta \cos(\theta/2) - 2 \sin(\theta/2)] \\ \sin(\theta/2) (2\delta + \rho^{1/3} \theta k) \end{bmatrix}, \quad (6)$$

$$\delta = \delta_0 + \delta_{csr} = \delta_0 + k\rho^{1/3}\theta. \quad (7)$$

Here the δ_0 and δ_{csr} indicate the particle’s initial energy deviation and CSR-induced energy deviation in the upstream dipoles, respectively. The δ_{csr} increases by $k\rho^{1/3}\theta$ right after experiencing the kick. The parameter k is relevant to the Gaussian bunch as [32]

$$k = 0.2459 \frac{N_b r_e}{\gamma \sigma_z^{4/3}}, \quad (8)$$

where N_b is the electron population, r_e is the classical electron radius, γ is the relativistic Lorentz factor. The rms bunch length σ_z , as a function of s , is the varying bunch length. For the following chicane calculation using the point-kick model, we assume that σ_z and the corresponding k are constant within a dipole and that each dipole has a different σ_z and k . Specifically, the bunch lengths in the 1st and 4th dipoles are equal to the bunch lengths at the chicane entrance and exit, respectively; the bunch lengths in the 2nd and 3rd dipoles are equal to the bunch lengths at the centers of the dipoles.

The emittance growth due to CSR can be suppressed by minimizing the CSR-induced coordinate shifts relative to the

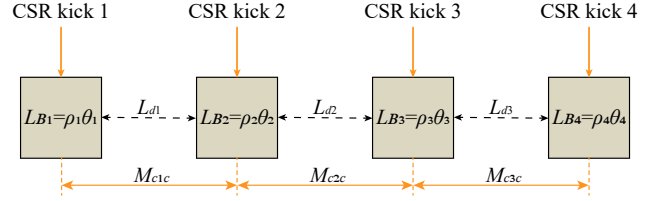


FIG. 1. Schematic of a chicane for the two-dimensional point-kick analysis of the CSR effect. The arrows point to the centers of the dipoles. M_{c1c} , M_{c2c} and M_{c3c} represent the transfer matrix from the center of 1st dipole to 2nd dipole, the center of 2nd dipole to 3rd dipole, and the center of 3rd dipole to 4th dipole, respectively.

reference trajectory at the chicane exit. This point is easily obtained from the expression of the transverse emittance in the presence at the exit of the beamline: [38]

$$\varepsilon_x^2 = \varepsilon_{x0}^2 + \varepsilon_{x0} \left(\beta_x \langle \Delta x_f'^2 \rangle + 2\alpha_x \langle \Delta x_f \Delta x_f' \rangle + \gamma_x \langle \Delta x_f^2 \rangle \right) + \Delta \varepsilon_x^2. \quad (9)$$

Here $\Delta \varepsilon_x^2 = \langle \Delta x_f^2 \rangle \langle \Delta x_f'^2 \rangle - \langle \Delta x_f \Delta x_f' \rangle^2 = 0$. Since the particle coordinate deviations Δx_f and $\Delta x_f'$ from CSR field are correlated, this term goes to 0 [39]. Here ε_{x0} is the geometric emittance at the entrance s_0 , and $\alpha_x, \beta_x, \gamma_x$ are the Twiss functions at the beamline exit.

Now we perform the 2D point-kick analysis of the four-bend chicane. To simplify the analysis, we assume a zero initial energy deviation of $\delta_0 = 0$ and a zero initial particle coordinates of $X_0 = (x_0, x'_0)^\dagger = (0, 0)^\dagger$ at the chicane entrance. After passing through the section from the center of 1st dipole to the center of 2nd dipole, the particle experiences the second kick,

$$X_{s2} = M_{c1c, 2 \times 2} X_{k1} + X_{k2}. \quad (10)$$

From the 2×2 transfer matrix of the horizontal betatron motion in Eqs. (2) and (3), the transfer matrix $M_{c1c, 2 \times 2}$ between the center of the first two dipoles is given by

$$M_{c1c, 2 \times 2} = (R_{HB2} R_{d1} R_{HB1})_{2 \times 2} = \begin{bmatrix} 1 & L_{d1} + (\theta_1 \rho_1 + \theta_2 \rho_2)/2 \\ 0 & 1 \end{bmatrix}, \quad (11)$$

where R_{HB1} and R_{HB2} are the transfer matrix of the 1st and 2nd half-dipoles, respectively. Note that Eq. (11) is a universal expression for (half dipole)+drift+(half dipole) structure, where one just needs to change the subscripts to obtain the matrix of other similar structure.

Similarly, the particle coordinate deviations after the 4th kick are

$$\begin{aligned} X_{s4} &= M_{c3c, 2 \times 2} X_{s3} + X_{k4} \\ &= M_{c3c, 2 \times 2} (M_{c2c, 2 \times 2} X_{s2} + X_{k3}) + X_{k4} \\ &= M_{c3c, 2 \times 2} M_{c2c, 2 \times 2} X_{s2} + M_{c3c, 2 \times 2} X_{k3} + X_{k4}. \end{aligned} \quad (12)$$

The description of $M_{c2c, 2 \times 2}$ and $M_{c3c, 2 \times 2}$ can be obtained by substituting the $\rho_1, \rho_2, \theta_1, \theta_2, L_{d1}$ in Eq. (11) with the counterparts $\rho_2, \rho_3, \theta_2, \theta_3, L_{d2}$ and $\rho_3, \rho_4, \theta_3, \theta_4, L_{d3}$, respectively.

Note that the net energy deviation δ_j increases by $k_j \rho_j^{1/3} \theta_j$ after passing through the j th dipole, which can be written as

$$\begin{aligned} \delta_1 &= k_1 \rho_1^{1/3} \theta_1, & \delta_2 &= \sum_{i=1}^2 k_i \rho_i^{1/3} \theta_i, \\ \delta_3 &= \sum_{i=1}^3 k_i \rho_i^{1/3} \theta_i, & \delta_4 &= \sum_{i=1}^4 k_i \rho_i^{1/3} \theta_i, \end{aligned} \quad (13)$$

respectively. Finally, the particle coordinate deviations X_f at the chicane exit are

$$X_f = (R_{HB4})_{2 \times 2} X_{s4} = \begin{bmatrix} X_{s4}(1, 1) + \frac{\theta_4 \rho_4}{2} X_{s4}(2, 1) \\ X_{s4}(2, 1) \end{bmatrix}, \quad (14)$$

where $X_{s4}(1, 1), X_{s4}(2, 1)$ are the elements of X_{s4} in Eq. (12). Therefore, the CSR-induced emittance growth at the chicane exit can be theoretically cancelled when the particle coordinate deviations satisfy $X_f = (0, 0)^\dagger$, which can also be written as $X_{s4} = (0, 0)^\dagger$.

Although the particle coordinate deviations in the chicane exit are obtained, it is of considerable complexity of the obtained X_{s4} . Therefore, a Taylor expansion is used to simplify the sine and cosine terms in X_{s4} with respect to the dipole bending angle θ_i ($i = 1, 2, 3, 4$), employing a small bending-angle approximation. Besides, we neglect the lengths of the dipoles as $L_B \ll L_d$. Whereby two analytical CSR cancellation conditions can be obtained in a greatly simplified form with the aid of the achromatic condition (Eq. (5)) as

$$\frac{q_2}{q_3 q_4 \ell_3} = \frac{\delta_4 - \delta_2}{\delta_2}, \quad \ell_2 = -\frac{1}{q_3} \frac{q_3(\delta_3 - \delta_1) + (q_2 + q_3)\delta_2}{\delta_2 + (1 + q_2)(\delta_3 - \delta_1)}, \quad (15)$$

where $q_2 = \theta_2/\theta_1, q_3 = \theta_3/\theta_1, q_4 = \theta_4/\theta_1, \ell_2 = L_{d2}/L_{d1}, \ell_3 = L_{d3}/L_{d1}$.

Although the CSR cancellation conditions in Eq. (15) look complicated, they still reveal some important information. First, Eq. (15) enable us to prove that a symmetric C-chicane seems cannot fully cancel the net CSR point-kick. Specifically, combined with these conditions for a symmetric C-chicane: $q_2 = q_3 = -1, q_4 = 1, \rho_1 = -\rho_2 = -\rho_3 = \rho_4$, and $\ell_3 = 1$, the first member of Eq. (15) can be reduced to $k_1 + k_2 = k_3 + k_4$. This condition cannot be satisfied, because k_i in Eq. (8) decreases as i increases during the compression process. Second, Eq. (15) also indicates that less than four dipoles is impossible to satisfy the CSR cancellation conditions. This is because, a chicane with three different dipoles, can be regarded as a four-bend chicane with one dipole's bending angle set to zero. Note that the first member of Eq. (15) cannot be satisfied regardless of arbitrary q_i ($i = 2, 3, 4$) set to zero. Self-evidently, one dipole can cause the CSR effect, and a compressor consisting of two different dipoles is not achromatic.

In total, it can be observed that there are *seven* degrees of freedom in a chicane, including $q_2, q_3, \rho_2/\rho_1, \rho_3/\rho_1, \rho_4/\rho_1, \ell_2$ and the compression factor C hidden in k_i . The not mentioned quantities q_4, ℓ_3 can be obtained from Eq. (5). Additionally, we need not care much about the values of the θ_1, ρ_1 and L_{d1} here, because the chicane design goals (including the total

length L_{tot} , the 1st dipole length L_{B1} and momentum compaction $R_{56}^{s0 \rightarrow sf}$) impose limits on the three variables. And the specific chicane layout can be realized by adjusting the ratios of other bending angles, other bending angles, and other drift lengths to θ_1, ρ_1 and L_{d1} , respectively. To illustrate the CSR cancellation conditions quantitatively, it is necessary to reduce the *seven* degrees of freedom to *three*. Then one can derive the chicane parameters as a function of compression factor C under the *two* CSR cancellation conditions in Eq. (15). Here we choose compression factor C as the independent variable in order to ensure the general applicability of our study. From the above analysis, we see that we need include *four* additional conditions for chicanes. Indeed, adding *four* conditions is not difficult because *three* conditions can be achieved just by ensuring that the four dipoles have either equal bending radii or equal dipole lengths. These two options are equivalent for the purpose of adding three conditions.

III. APPLICATION TO FOUR-BEND C-CHICANE

Currently, the symmetric C-chicane is the most commonly used bunch compressor in operation or under construction. Thus we hope to discuss the implementation of a chicane based on a symmetric C-chicane as much as possible. At this point, we make the bending angles of the 1st dipole and 2nd dipole identical except for the bending direction (denoted as $\theta_1 = -\theta_2$ or $q_2 = -1$). The schematic layout is shown in Fig. 2. This condition $q_2 = -1$ preserves the parallelism of the beam orbits between the 2nd and 3rd dipoles, indicating a similarity with the symmetric C-chicane. The condition $q_2 = -1$ also results in θ_3 being equal to $-\theta_4$. This greatly simplifies the structure of the chicane, reducing the four different dipoles to only two types. Importantly, the condition $q_2 = -1$ also greatly simplifies the achromatic condition and CSR cancellation conditions. First, the achromatic condition in Eq. (5) can rewrite as

$$q_4 = -q_3, \quad \ell_3 = -1/q_3. \quad (16)$$

Substituting the above Eq. (16) in Eq. (15), the CSR cancellation conditions can be reduced to

$$-\frac{1}{q_3} = \frac{\delta_4 - \delta_2}{\delta_2}, \quad \ell_2 = -\frac{\delta_3 - \delta_1}{\delta_2} + \frac{1}{q_3} - 1. \quad (17)$$

Note that the second member of Eq. (17) turns out that $\ell_2 = L_{d2}/L_{d1}$ is negative due to the negative q_3 and the positive $\delta_3 - \delta_1, \delta_2$. Despite the presence of “negative drift”, we note that the dispersion and the beam trajectory remain unaffected, since Eqs. (4) and (5) show the independence of L_{d2} under the condition of $q_2 = -1$. Indeed, this “negative drift” is not uncommon in accelerator physics and can be realized by using a focus section with several quadrupoles and drifts [45]. For clarity, in this section we use $L_{d2}^{\text{real}}(\ell_2^{\text{real}})$ to describe the real length of the physical space, and $L_{d2}^{\text{eff.}}(\ell_2^{\text{eff.}})$ for a focus section whose transfer matrix is the same as that of a “negative drift”.

Together with the condition $q_2 = -1$, two typical cases of fixed bending radii and fixed dipole lengths are discussed to

provide *four* conditions, which can be expressed as

Case 1: $q_2 = -1$, $\rho_2/\rho_1 = -1$, $\rho_3/\rho_1 = -1$, $\rho_4/\rho_1 = 1$.

Case 2: $q_2 = -1$, $\rho_2/\rho_1 = -1$, $\rho_3/\rho_1 = 1/q_3$, $\rho_4/\rho_1 = -1/q_3$.
(18)

These two cases correspond to two scenarios: Case 1 is given priority during the chicane design phase, where the bending radii are fixed by setting the equal magnetic field B_0 ; Case 2 is typically used for pre-manufactured dipoles, allowing for adjustment of the dipole's bending angles by changing B_0 .

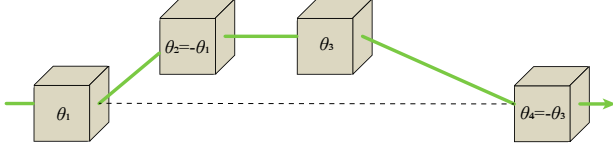


FIG. 2. General geometry of an asymmetric C-chicane. The space between the 2nd and 3rd dipoles is parallel to the entrance or exit of the beam, which is a “negative drift” constructed by several quadrupoles.

A. CSR-immune asymmetric C-chicane

For Case 1, bending radii are fixed value as $|\rho_1| = |\rho_2| = |\rho_3| = |\rho_4|$. By substituting the k_i ($i = 1, 2, 3, 4$) (as presented in Appendix A) in Eq. (17), the CSR cancellation conditions for a CSR-immune chicane can be written as

$$C^{-4/3} + \left[\frac{2(1-q_3)}{1+C-2Cq_3} \right]^{4/3} = q_3^2 \left\{ 1 + \left[\frac{2(1-q_3)}{2-q_3-Cq_3} \right]^{4/3} \right\}, \quad (19)$$

and

$$\ell_2^{\text{eff.}} = -1 + \frac{1}{q_3} - \frac{[2C(1-q_3)]^{4/3}}{(C-2Cq_3+1)^{4/3} + [2C(1-q_3)]^{4/3}} + \frac{2^{4/3}}{q_3 \left\{ \left[\frac{2-(1+C)q_3}{1-q_3} \right]^{4/3} + 2^{4/3} \right\}}. \quad (20)$$

Since Eqs. (19) and (20) are too complicated for analytical solutions, one can obtain the numerical results of q_3 vs. C and $\ell_2^{\text{eff.}}$ vs. C from Eqs. (19) and (20). The corresponding quantities q_4 vs. C and ℓ_3 vs. C can be found from the solved q_3 vs. C , since $q_4 = -q_3$, $\ell_3 = -1/q_3$. Figure 3 shows that the solved q_3 ($\ell_2^{\text{eff.}}$) is equal to -1 (-3) for no compression case ($C = 1$), and decreases as the compression factor C increases. Indeed, approximate but explicit expressions of q_3 and $\ell_2^{\text{eff.}}$ can also be obtained by fitting the numerical results for factor $C < 25$ as

$$q_3 \approx -C^{-1/2}, \quad \ell_2^{\text{eff.}} \approx -1 - 2C^{0.39}. \quad (21)$$

The comparison between the approximate and theoretical results is shown in Fig. 3 by the dashed and solid curves. Importantly, Eq. (19) (or Fig. 3, upper plot) indicates that shortening the dipole lengths of the last two dipoles is necessary

to achieve a CSR-immune chicane. This point can be understood qualitatively as the bunch length is shorter at the last two dipoles, where CSR is stronger.

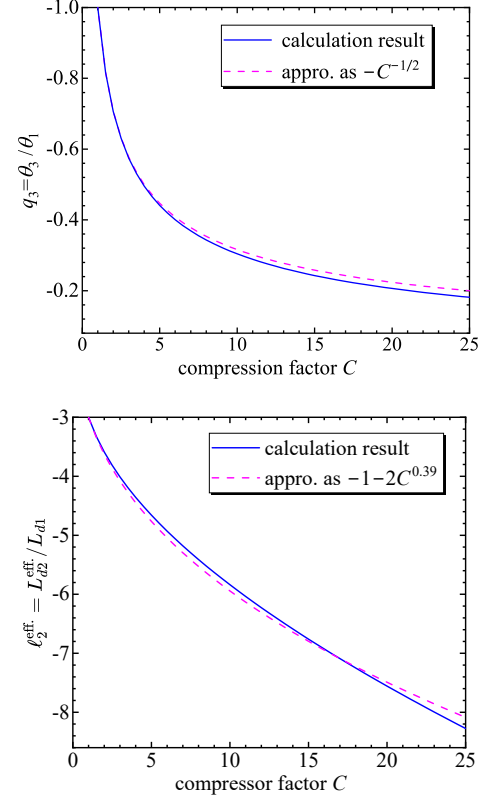


FIG. 3. The required bending angles ratio $q_3 = \theta_3/\theta_1$ (upper) and ratio $\ell_2^{\text{eff.}} = L_{d2}^{\text{eff.}}/L_{d1}$ (bottom) vary with the compression factor C from CSR cancellation conditions Eqs. (19) and (20) (blue solid curves) for Case 1. The pink dashed curves show simpler expression $q_3 \approx -C^{-1/2}$ and $\ell_2^{\text{eff.}} \approx -1 - 2C^{0.39}$, respectively.

For Case 2, the dipole lengths satisfy $L_{B1} = L_{B2} = L_{B3} = L_{B4}$. Similarly to Case 1, we obtain the empirical equations of q_3 and $\ell_2^{\text{eff.}}$ for the factor $C < 25$ as

$$q_3 \approx -C^{-3/5}, \quad \ell_2^{\text{eff.}} \approx -1 - 2C^{0.47}, \quad (22)$$

for the case of fixed dipole lengths. From Eq. (22), it can be seen that the key to achieving a CSR-immune chicane, as already described in Ref. [24], is to weaken the last two dipoles compared with a traditional symmetric C-chicane. However, the parameter scans and particle tracking approach in Ref. [24] works only in a case-by-case sense. Here we present a general demonstration rather than focusing on a practical design.

Finally, the chicane design goal, the $R_{56}^{s_0 \rightarrow s_f}$ and L_{tot} , can be obtained from the value of L_{d1} , θ_1 , and the provided q_3 (see Figs. 3 and 4 (upper)) as

$$R_{56}^{s_0 \rightarrow s_f} = -L_{d1}\theta_1^2(1-q_3), \quad L_{\text{tot}} = L_{d2}^{\text{real}} + L_{d1}(1-1/q_3), \quad (23)$$

which indicates that for a given design goal and a larger compression factor C (that is, a smaller $|q_3|$), there will be a smaller

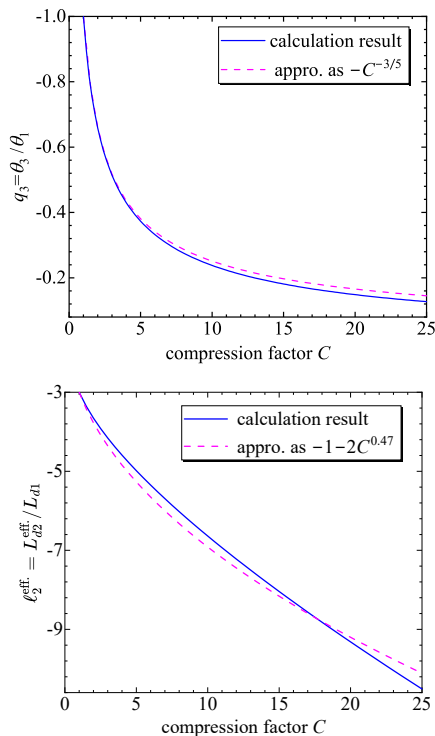


FIG. 4. The required bending angles ratio $q_3 = \theta_3/\theta_1$ (upper) and ratio $\ell_2^{\text{eff}} = L_{d2}^{\text{eff}}/L_{d1}$ (bottom) vary with the compression factor C from CSR cancelation conditions for Case 2 (blue solid curves). The pink dashed curves show simpler expression $q_3 \approx -C^{-3/5}$ and $\ell_2^{\text{eff}} \approx -1 - 2C^{0.47}$, respectively.

L_{d1} and a larger θ_1 , and vice versa. This conclusion also applies to the comparison with the traditional C-chicane, which is the case of $|q_3|=1$. Our proposed asymmetric design have larger $|\theta_1|$, L_{d3} and smaller $|\theta_3|$, L_{d1} , compared with symmetric C-chicane with the same design goal.

B. Numerical verification of the proposed conditions

In the above subsection, we have obtained generic CSR cancelation conditions for an asymmetric C-chicane. However, these conditions in Eq. (17) are derived under two assumptions: the variation in bunch length within a single dipole is not considered, and the lengths of the dipoles are neglected. Therefore, the main purpose of this subsection is to investigate the value of $(q_3, \ell_2^{\text{eff}})$ using more precise calculations, and then to compare it with the result from the point-kick model. Both numerical integration method and ELEGANT particle tracking simulations are performed.

To this end, the dipole lengths are further taken into account in the calculation of the parameters of $R_{56}^{s_0 \rightarrow s_f}$, L_{tot} , and ℓ_3 with aid of the Eq. (4) (see Appendix B). For the convenience of comparison, all chicanes analyzed in this study have been assigned the same values for L_{tot} , $R_{56}^{s_0 \rightarrow s_f}$, L_{B1} , and compression factor C . For numerical integration, we need to specify the concrete value of these consistent quantities during calcula-

TABLE I. Parameters common to all bunch compressor chicanes compared in this paper.

	Symbol	chicane Parameters	Unit
Total length	L_{tot}	20	m
First-order momentum compaction	$R_{56}^{s_0 \rightarrow s_f}$	37.5	mm
Compression factor	C	10	—
Length of the 1st dipole	L_{B1}	1.0	m

TABLE II. Parameters of the symmetric and asymmetric C-chicane settings for Case 1 with units in meters.

	Symbol	symmetric C-chicane	asymmetric C-chicane
Length of the first two dipoles	L_{B1}, L_{B2}	1.0	1.0
Length of the last two dipoles	L_{B3}, L_{B4}	1.0	0.30
Bending radii of each dipole	ρ	18.86	10.07
Length of the 1st drift	L_{d1}	5.5	2.17
Length of the 3rd drift	L_{d3}	5.5	10.23
Effective value of the 2nd drift	L_{d2}^{eff}	—	-20.65

tion. We set a design based on a symmetric C-chicane with typical parameters of equal dipole length of 1 m, the 1st and 3rd drift lengths of 5.5 m, the length between the 2nd and 3rd dipoles of 5 m, bending angles of 3.0° , and the compression goal of $C = 10$. Such chicane parameters enable the derivation of the complete information for a symmetric C-chicane, as listed in Tables I and II. The design goals in Table I are common to all chicanes compared in the following.

Now we verify the theoretical result of the point-kick model. The CSR-induced coordinate deviations are evaluated using a numerical integration method [38], which can be considered as a bunch length variation model within each dipole. The verification for our calculation is similar to Ref. [36], and the details are presented in Appendix C. From Eqs. (19) and (20), we can obtain the theoretical values of $(q_3^*, \ell_2^{\text{eff},*}) = (-0.30, -5.84)$ for a bunch compressed by a factor of 10. Here we consider a chicane case with the parameters the same as those listed in Table I, and a physical length of $L_{d2}^{\text{real}} = 5$ m, which is designed to accommodate quadrupoles. According to the integration method, the calculation results of $(\ell_2^{\text{eff}}/\ell_2^{\text{eff},*}, q_3/q_3^*) = (1.770, 0.881)$ can be derived from $|\Delta x_f| = 0$ m and $|\Delta x'_f| = 0$, as shown in the pink pentacle in Fig. 5. Here ℓ_2^{eff} and q_3 are normalized with respect to $\ell_2^{\text{eff},*}$ and q_3^* just for clear comparison. This result $(\ell_2^{\text{eff}}/\ell_2^{\text{eff},*}, q_3/q_3^*)$ close to (1, 1) indicates a accurate calculation by the point-kick model. As shown, the point-kick analysis results and integration results are slightly different but basically consistent.

The integration results indicate that the value of q_3 is independent of ℓ_2^{eff} , as shown in the red curves in Fig. 5. This is not the first time that independence has been achieved, and the previous point-kick analysis also highlighted this situation

TABLE III. The initial and final beam parameters for the ELEGANT simulations.

beam Parameters	Symbol	Value	Unit
Bunch charge	Q	300	pC
Initial rms bunch length	σ_{z0}	100	μm
Beam energy	E_0	3	GeV
Norm. transv. emittance	ε_{n0}	0.9	$\mu\text{m}\cdot\text{rad}$
Rel. rms energy spread	σ_δ	0.01	%

(see Eq.(19)). This independence can be attributed to the fact that the expression of Δx_f^2 in Eqs. (44) does not have L_{d2}^{eff} and depends solely on q_3 (see Eqs. (45)-(48)). From this perspective, we find that the CSR-induced coordinate deviation $\Delta x_f' = 0$ can be achieved simply by adjusting the deflection magnitude (or dipole length) of the last two dipoles and the first two with a ratio of q_3 .

In the numerical verification above, we find that the deviations of the obtained (ℓ_2, q_3) with respect to the model calculation, can be attributed to the set ratio between L_{B1} and $(L_{\text{tot}} - L_{d2}^{\text{real}})$. As this ratio decreases, $(\ell_2^{\text{eff}}, q_3)$ become closer to the theoretical results $(\ell_2^{\text{eff},*}, q_3^*)$, as illustrated in Fig. 5. Although the point-kick analysis requires some fine-tuning, the differences are minor and can be compensated by parameter adjustments in the actual design process. Note that the integration methods and the following particle tracking, can yield more accurate results, however it is almost impossible to attain an analytical solution for the compression progress.

On the other hand, to verify the proposed CSR cancellation conditions, we simulated the emittance growth caused by steady-state CSR using ELEGANT [47, 48]. The Gaussian bunch with typical initial parameters is tracked as listed in Table III. The momentum chirp is set as $h = (1-C)/(CR_{56}^{s_0 \rightarrow s_f}) = 24.02 \text{ m}^{-1}$ from the values of compressor factor and $R_{56}^{s_0 \rightarrow s_f}$ in Table I. Here the initial Twiss parameters are scanned to minimum the emittance growth at the chicane exit by optimally matching the beam envelope to the orientation of a nonzero net CSR kick at the chicane exit [31]. Fig. 6 shows the simulations result of the CSR-induced emittance ε_n near $(q_3^*, \ell_2^{\text{eff},*})$. We can see that the minimum emittance growth $\Delta\varepsilon_n/\varepsilon_n$ is of 0.53% and the corresponding values are of $(q_3/q_3^*, \ell_2^{\text{eff}}/\ell_2^{\text{eff},*}) = (0.99, 1.63)$. These simulation results are close to the results of the point-kick analysis and basically agree with the integration results. With aid of the common chicane parameters in Table I and the scanned values (ℓ_2, q_3) , the complete chicane information can be obtained, as listed in Table II.

IV. APPLICATION TO FOUR-BEND S-CHICANE

We define the symmetric S-chicane as one in which the 1st and 4th dipoles have equal dipole length and the 2nd and 3rd dipoles are of double that, and all dipoles have the same bending strength, otherwise it is called asymmetric. And the symmetric S-chicane satisfies the position conditions that

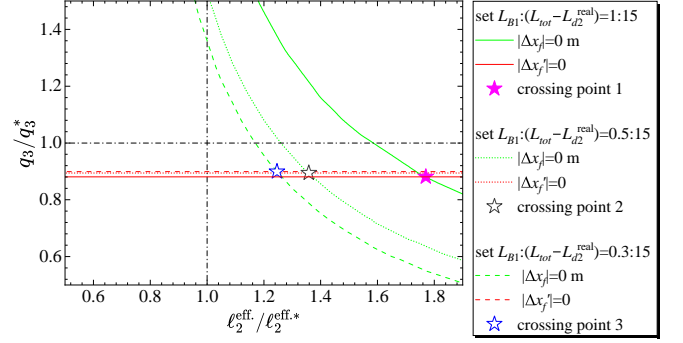


FIG. 5. The $(\ell_2^{\text{eff}}/\ell_2^{\text{eff},*}, q_3/q_3^*)$ of a chicane with $|\Delta x_f| = 0 \text{ m}$ and $|\Delta x_f'| = 0$, as shown in the green and red solid curves. The pink pentacle is the crossing point of the two curves. As a comparison, the results for $L_{B1}:(L_{\text{tot}} - L_{d2}^{\text{real}}) = 1.0:15, 0.5:15$ and $0.3:15$, are calculated as $(\ell_2^{\text{eff}}/\ell_2^{\text{eff},*}, q_3/q_3^*) = (1.770, 0.881), (1.358, 0.894)$ and $(1.246, 0.899)$, respectively.

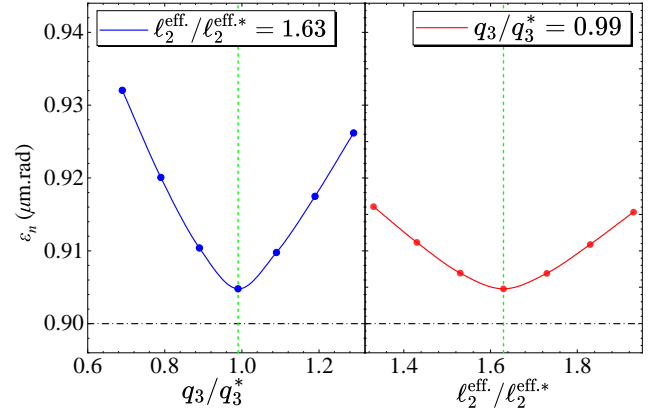


FIG. 6. The ELEGANT simulations result of the CSR-induced emittance ε_n near $(q_3^*, \ell_2^{\text{eff},*})$ for asymmetric C-chicane. The simulations results turn out that the parameters satisfy $(q_3/q_3^*, \ell_2^{\text{eff}}/\ell_2^{\text{eff},*}) = (0.99, 1.63)$ with scanned initial Twiss parameters $(\alpha_{x0}, \beta_{x0}) = (-2, 10 \text{ m})$, as shown in the green dashed curves.

$L_{\text{tot}} = 4L_{d1} = 2L_{d2} = 4L_{d3}$. In this section, we discuss the implementation of an asymmetric chicane based as much as possible on the symmetric one, while comparing the performance of the symmetric and asymmetric chicanes as a reference for our discussion.

Although S-chicanes are used less frequently than C-chicanes in FELs, existing studies shows that S-like chicanes exhibit a notable ability to preserve CSR-induced emittance [24, 42, 44, 46]. The utilization of five or six dipoles is required in such S-like chicanes. In Sec. IV A, we demonstrate a more ambitious idea of achieving a CSR-immune chicane using only *four* dipoles. The analysis reveals that such chicane has an S-type geometry as well and shows that four dipoles are enough to minimize the CSR effects for a chicane (shown in Fig. 7).

To further fulfil a CSR-immune chicane, *four* additional conditions (as introduced in the end of Sec. II B) are necessary. Firstly, two typical cases are discussed for chicane

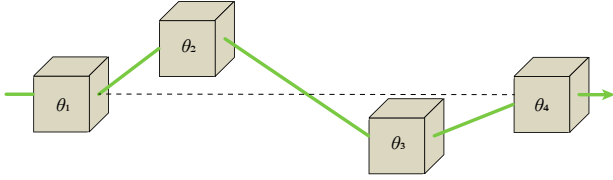


FIG. 7. General geometry of an asymmetric S-chicane. The drift length between the 1st and 2nd dipoles is a quarter of the chicane total length.

designs. Similar to Sec. III, Case 3 and Case 4 denote two chicanes for each dipole with fixed bending radii and fixed dipole lengths, respectively. Nevertheless, the current provided *three* conditions are insufficient, unless an additional condition is added. To mimic the structure of a symmetric S-chicane, the ratio $L_{d1}/L_{tot} = 1/4$ is set to be similar to a symmetric S-chicane. The ratio $L_{d1}/L_{tot} = 1/4$ allows the longitudinal positions of 1st, 2nd and 4th dipoles to be fixed, when the total length is constant. It should be pointed out that, although not strictly necessary, we set this position restrict for practical reasons. Because adjusting dipole positions can be more difficult than bending angles. Combined with the achromatic condition in Eq. (5) and the additional condition $L_{d1}/L_{tot} = 1/4$, the variables $q_4 = \theta_4/\theta_1$, $\ell_2 = L_{d2}/L_{d1}$, $\ell_3 = L_{d3}/L_{d1}$ can be expressed in terms of q_2, q_3 as

$$q_4 = -(1 + q_2 + q_3), \quad \ell_2 = \frac{4}{q_3} + 3\left(\frac{q_2}{q_3} + 1\right), \quad \ell_3 = -\frac{4}{q_3} - \frac{3q_2}{q_3}. \quad (24)$$

Together with the position condition $L_{d1}/L_{tot} = 1/4$, the *four* conditions can be expressed as

Case 3: $L_{d1}/L_{tot} = 1/4$, $\rho_2/\rho_1 = -1$, $\rho_3/\rho_1 = 1$, $\rho_4/\rho_1 = -1$.

Case 4: $L_{d1}/L_{tot} = 1/4$, $\rho_2/\rho_1 = 1/q_2$, $\rho_3/\rho_1 = 1/q_3$,

$$\rho_4/\rho_1 = 1/q_4. \quad (25)$$

The detailed design is introduced in Sec. IV B. The verifications of the CSR cancelation conditions by the integration method and numerical tracking via ELEGANT are given in Sec. IV C.

A. The proof of S-chicane with three positive drifts

The possibility of three positive drifts between dipoles is demonstrated in this subsection. The first member of Eq. (5) and the second member of Eq. (15) can be combined to yield the expression of ℓ_3 . Thus the expressions of ℓ_2 and ℓ_3 can be written as

$$\begin{aligned} \ell_2 &= -\frac{1}{q_3} \frac{q_3(\delta_3 - \delta_1) + (q_2 + q_3)\delta_2}{\delta_2 + (1 + q_2)(\delta_3 - \delta_1)}, \\ \ell_3 &= \frac{1}{q_3} \frac{q_2\delta_2}{\delta_2 + (1 + q_2)(\delta_3 - \delta_1)}. \end{aligned} \quad (26)$$

Our objective is to ensure that both ℓ_2 and ℓ_3 are positive. Note that $\delta_3 - \delta_1$ and δ_2 are both positive. As the signs of q_2 and q_3

are unknown, they can be classified into four groups based on their signs:

Group 1: set $q_2 > 0$ and $q_3 > 0$. This group is not applicable because $\ell_2 < 0$.

Group 2: set $q_2 > 0$ and $q_3 < 0$. This group is not applicable because $\ell_3 < 0$.

Group 3: set $q_2 < 0$ and $q_3 < 0$. As $\ell_3 > 0$, one can obtain $\delta_2 + (1 + q_2)(\delta_3 - \delta_1) > 0$. Thus $q_3(\delta_3 - \delta_1) + (q_2 + q_3)\delta_2 > 0$ as $\ell_2 > 0$. However, $q_3(\delta_3 - \delta_1) + (q_2 + q_3)\delta_2 > 0$ is impossible as $q_2 < 0, q_3 < 0$.

Group 4: set $q_2 < 0$ and $q_3 > 0$. The case that $\ell_2 > 0$ and $\ell_3 > 0$ is possible under the condition that $q_3(\delta_3 - \delta_1) + (q_2 + q_3)\delta_2 > 0$ and $\delta_2 + (1 + q_2)(\delta_3 - \delta_1) < 0$. Thus the result $1 + q_2 < 0$ can be achieved.

Up to now, we have excluded all possibilities based on the taxonomy, except for Group 4.

Lastly, the sign of q_4 can be determined by reusing the first member of Eq. (15), which turns out to be a negative q_4 . Taken as a whole, a chicane with three positive drifts must satisfy

$$q_2 < 0, \quad q_3 > 0, \quad q_4 < 0, \quad 1 + q_2 < 0, \quad \frac{\delta_3 - \delta_1}{\delta_2} > -\frac{1}{1 + q_2}. \quad (27)$$

One can find that it can be identified as an S-chicane (Fig. 7) from the angle relation. And the test indicates that the last condition in Eq. (27) is achievable, e.g., by adjusting the bending radii $\rho_i (i = 1, 2, 3)$ in $\delta_3 - \delta_1$ and δ_2 .

B. CSR-immune asymmetric S-chicane

For Case 3, the bending radii are set to $\rho_1 = -\rho_2 = \rho_3 = -\rho_4$. Given the complexity of the obtained CSR cancelation conditions in Eq. (15) (see Appendix A), we calculate the results of $q_2 = \theta_2/\theta_1, q_3 = \theta_3/\theta_1$ in terms of the compression factor C , as shown in Fig. 8. Using the obtained q_2 and q_3 , we also compute the values of q_4, ℓ_2, ℓ_3 from Eq. (24) as shown in Figs. 8 and 9, which varies only with compression factor C .

For Case 4, the dipole lengths are fixed as $L_{B1} = L_{B2} = L_{B3} = L_{B4}$. In a similar manner to Case 3, the values of q_2, q_3 can be solved from Eqs. (15) and (24) under the conditions in Eq. (25). Correspondingly, the quantities q_4, ℓ_2, ℓ_3 for Case 4 are plotted in Figs. 10 and 11. We observe that the results of $q_2, q_3, q_4, \ell_2, \ell_3$ in Case 4 shows great similarity with those of Case 3.

We find that, the theoretical results for both Case 3 and Case 4 indicate that the last two dipoles are weaker (shorter) than the first two dipoles for the asymmetric S-chicane. More specifically, the 3rd (4th) dipole is shorter or weaker than the 2nd (1st) dipole for Case 3 or Case 4, respectively. This weakening or shortening effect becomes more pronounced as the compression factor increases. We also find that a symmetric S-chicane fails to satisfy the CSR cancelation conditions in our calculation, as none of the compression factors C in Figs. 8 and 10 meet the requirement that both $q_2 = -2$ and $q_3 = 2$.

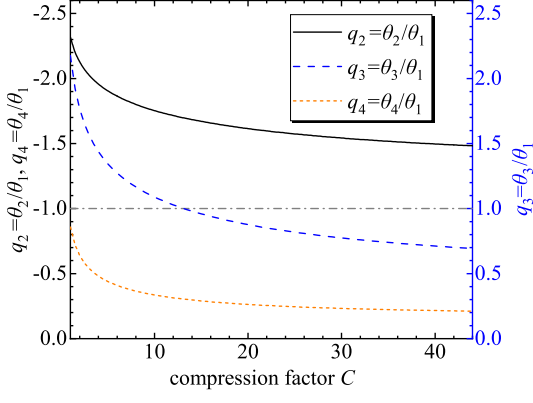


FIG. 8. The solved $q_2 = \theta_2/\theta_1, q_3 = \theta_3/\theta_1$ from Eqs. (15), (24) in terms of compression factor C for Case 3. The corresponding $q_4 = \theta_4/\theta_1$ is also included. The black dashed curve is plotted for clear comparison with q_2, q_3, q_4 .

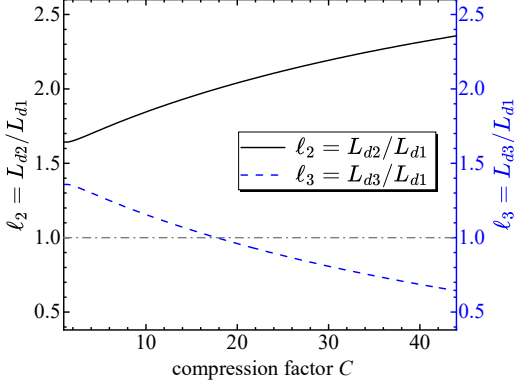


FIG. 9. The corresponding $\ell_2 = L_{d2}/L_{d1}, \ell_3 = L_{d3}/L_{d1}$ after solving the $q_2 = \theta_2/\theta_1$, and $q_3 = \theta_3/\theta_1$ for Case 3. The black dashed curve is plotted for clear comparison with ℓ_2 and ℓ_3 .

C. Numerical verification of the proposed conditions

To investigate the impact of the assumptions, including the constant bunch length in one dipole and the neglected dipole length, we perform numerical integration and ELEGANT analysis for the asymmetric S-chicane. To begin with, we present the results of the numerical integration. First, the dipole lengths are taken into account. The expressions of ℓ_2, ℓ_3 in Eq. (26) and the $R_{56}^{s_0 \rightarrow s_f}, L_{tot}$ are recalculated, the details of which can be found in Appendix B. Second, we consider a gradually varying bunch length in a similar manner to the asymmetric C-chicane using an integration method [38]. These variables $R_{16}^{s \rightarrow s_f}$ and $R_{26}^{s \rightarrow s_f}$ in Eq. (44), and $R_{56}^{s_0 \rightarrow s}$ in k_1, k_2, k_3, k_4 , change with the position s , as expressed in Appendix C. Eventually, the CSR cancelation conditions can be obtained and compared with the results $q_2^* = -1.75, q_3^* = 1.09$ (Eq. (15)) for Case 3 when the compression factor is $C = 10$. Figure 12 (pink pentacle) shows the results from integration method as $(q_2/q_2^*, q_3/q_3^*) = (0.947, 0.859)$, indicating a relatively accurate calculation of the point-kick model. Similar

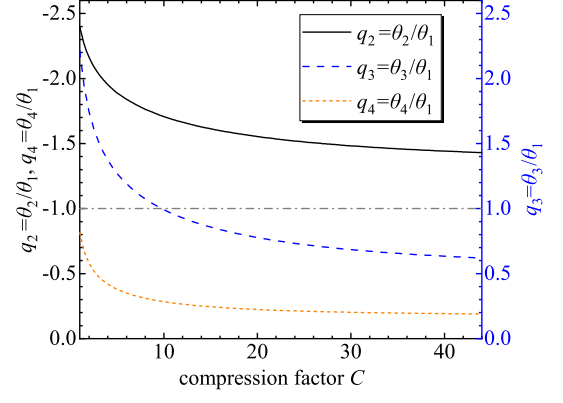


FIG. 10. The solved $q_2 = \theta_2/\theta_1, q_3 = \theta_3/\theta_1$ from Eqs. (15), (24) in terms of compression factor C for Case 4. The corresponding $q_4 = \theta_4/\theta_1$ is also included. The black dashed curve is plotted for clear comparison with q_2, q_3, q_4 .

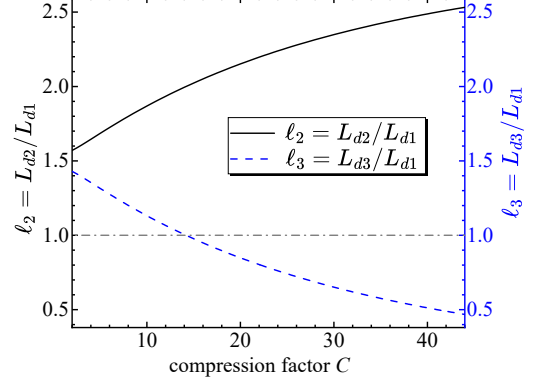


FIG. 11. The corresponding $\ell_2 = L_{d2}/L_{d1}, \ell_3 = L_{d3}/L_{d1}$ after solving the $q_2 = \theta_2/\theta_1$, and $q_3 = \theta_3/\theta_1$ for Case 4. The black dashed curve is plotted for clear comparison with ℓ_2 and ℓ_3 .

to the asymmetric C-chicane, the (q_2, q_3) obtained by integration method is closer to the result of the point-kick model after reducing the ratio $L_{B1} : L_{tot}$, as shown in Fig. 12.

Furthermore, the minimum transverse emittance ε_n for the asymmetric S-chicane, together with the corresponding (q_2, q_3) , is searched via ELEGANT simulations. The scanned results $(q_2/q_2^*, q_3/q_3^*) = (0.94, 0.86)$ are obtained. For illustration, the normalized emittance growth near $(q_2/q_2^*, q_3/q_3^*)$ is displayed in Fig. 13. Correspondingly, the complete asymmetric S-chicane information can be found in Table IV. Our results from point-kick analysis are consistent with these numerical results basically.

V. COMPARISON AMONG SYMMETRIC AND ASYMMETRIC C- AND S-CHICANES

In this section, to further demonstrate the CSR suppression efficiency of our proposed asymmetric chicane designs, we compare the performance in suppressing the CSR-induced

TABLE IV. Parameters of the symmetric and asymmetric S-chicane settings for Case 3 with units in meters.

	Symbol	symmetric S-chicane	asymmetric S-chicane
Bending radii of each dipole	ρ	20.66	14.46
Length of the 2nd dipole	L_{B2}	2.0	1.65
Length of the 3rd dipole	L_{B3}	2.0	0.94
Length of the 4th dipole	L_{B4}	1.0	0.29
Length of the 1st drift	L_{d1}	3.25	3.18
Length of the 2nd drift	L_{d2}	7.5	8.10
Length of the 3rd drift	L_{d3}	3.25	4.85

emittance growth among the four types of chicanes, including symmetric C- and S-chicanes, and the asymmetric C- and S-chicanes. These chicanes have set the same L_{tot} , $R_{56}^{s_0 \rightarrow s_f}$, L_{B1} , and compression factor C , as summarized in Table I. Whereby one can obtain the other chicane parameters of symmetric S-chicane, as presented in Table IV. These chicanes are tested by ELEGANT with the initial bunch parameters in Table III.

By scanning the initial C-S parameters, we aim to achieve minimum emittance growth at the exit of the symmetric C- and S-chicanes. By doing this, the simulation results for every chicanes can be obtained by ELEGANT and can be seen in Table V. In the case of the asymmetric C- and S-chicanes, the normalized emittance growth $\Delta\epsilon_n/\epsilon_{n0}$ is reduced by more than tenfold compared with the symmetric ones. It appears that the emittance growth due to CSR can be effectively suppressed.

In the above sections, the emittance growths induced by dipole-CSR have been verified for asymmetric C- and S-chicanes. However, some study has shown that a longer drift space between the dipoles may degrade the emittance significantly, as the CSR effects dominate in the drift space [5].

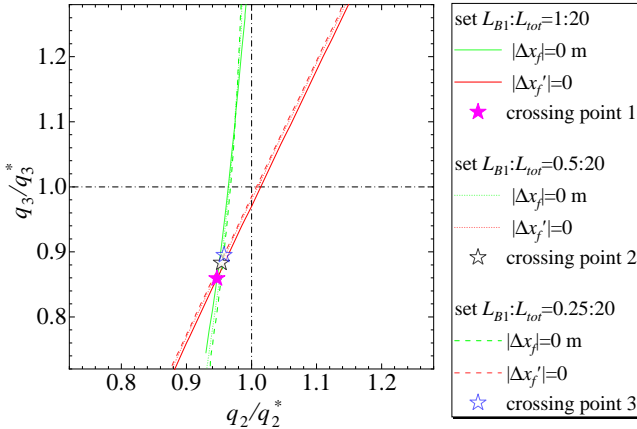


FIG. 12. The $(q_2/q_2^*, q_3/q_3^*)$ of a chicane with $|\Delta x_f| = 0$ m and $|\Delta x_f'| = 0$, as shown in the green and red solid curves. As a comparison, the result for $L_{B1} : L_{d1} = 1:20, 0.5:20$ and $0.25:20$ are calculated as $(q_2/q_2^*, q_3/q_3^*) = (0.947, 0.859), (0.954, 0.883),$ and $(0.958, 0.895)$, respectively.

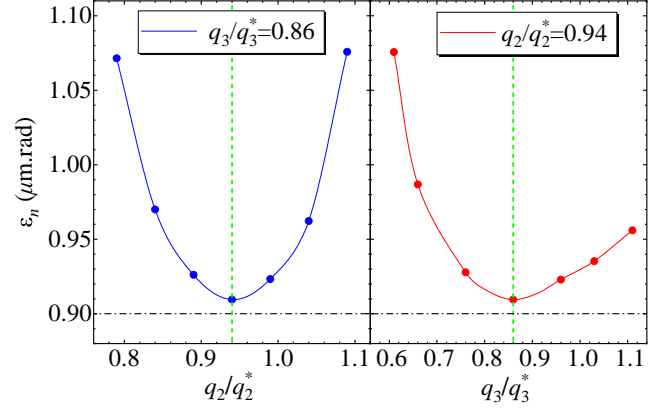


FIG. 13. The ELEGANT simulations result of the CSR-induced emittance ϵ_n near (q_2^*, q_3^*) for asymmetric S-chicane. The simulation results turn out that the parameters satisfy $(q_2/q_2^*, q_3/q_3^*) = (0.94, 0.86)$ with scanned initial Twiss parameters $(\alpha_{x0}, \beta_{x0}) = (1.5, 32$ m), as shown in the dashed curves.

TABLE V. Results of the ELEGANT simulations of the finally geometric emittance ϵ_{nf} , and relative emittance growth $\Delta\epsilon_n/\epsilon_{n0}$ for symmetric and asymmetric C- and S-chicane with initial emittance $\epsilon_{n0} = 0.9$ $\mu\text{m.rad}$.

CSR effects	ϵ_{nf} ($\mu\text{m.rad}$)	$\Delta\epsilon_n/\epsilon_{n0}$
asymmetric C-chicane		
steady-state CSR	0.905	0.53%
all-CSR	0.962	6.86%
symmetric C-chicane		
steady-state CSR	1.0	11.0%
all-CSR	1.238	37.6%
asymmetric S-chicane		
steady-state CSR	0.910	1.1%
transient CSR	0.950	5.55%
symmetric S-chicane		
steady-state CSR	1.096	21.8%
transient CSR	1.344	49.3%

Therefore, it is worthwhile to investigate more detail CSR effects (denoted by all-CSR), considering the transient CSR at the dipole edges, incoherent synchrotron radiation in the bending magnets, the classical, single-particle synchrotron radiation, and the CSR effect in the dipoles and the following drift space with the Stupakov model [47]. Furthermore, we simulate the emittance growth of the symmetric (asymmetric) C- and S-chicanes, taking into account the all-CSR effects. The results are listed in Table V. We find that the relative emittance growth of the symmetric C- and S-chicanes are 5.5 and 8.9 times larger than that of asymmetric ones, respectively. Overall, the asymmetric C- and S-chicanes have good success in suppressing of the emittance growth, whether only the dipole-induced CSR or the all-CSR is considered.

VI. SUMMARY AND DISCUSSION

This paper reports an analytical expression of the CSR net kick, thus finds a solution to cancel the CSR-induced transverse emittance growth in a chicane. The theoretical CSR cancellation conditions, derived from the point-kick model, indicate an asymmetric chicane design for both C and S chicane geometries. The design of the asymmetric C-chicane may be valuable for improving on the current numerous symmetric C-chicanes. Specifically, it is required to adjust the bending angle ratio between the first two dipoles and the last two, as well as the length ratio between the 1st and 3rd drifts. Despite the presence of a “negative drift” between the 2nd and 3rd dipoles, this can be realized by adding quadruples in 2nd drift section. Correspondingly, the ratio q_3 and the effective value of the “negative drift” can be approximated to be a simpler expression as Eqs. (21) and (22). For the asymmetric S-chicane, the 1st and 3rd (2nd and 4th) dipoles have the same bending direction. The chicane information, including the bending angles and draft length ratios, are shown in Figs. 8, 9 and 10, 11 for the cases of fixed bending radii and fixed dipole lengths, respectively. Roughly, both the values of $(\theta_3/\theta_1, L_{d2}^{\text{eff}}/L_{d1})$ for C-chicane and $(\theta_2/\theta_1, \theta_3/\theta_1)$ for S-chicane can be determined as compression factor C -dependent quantities. Such a property enables our results easily transferable to arbitrary chicane design.

As a verification of these theoretical results, numerical integration calculations and ELEGANT simulations for asymmetric C- and S-chicanes are presented, which show a slight shift with respect to the theoretical result. However our result remains valuable as it reveals the main picture of cancelling the CSR-driven emittance excitation. For an actual design, the theoretical results can be considered as initial values and then the design can be optimized by fine-tuning the chicane parameters. Moreover, compared with the symmetric C- and S-chicanes with the same compression target, the proposed asymmetric chicanes, show a promising performance in suppressing the emittance growth in our simulations.

One can find that the key to suppressing the CSR effect is to weaken the strengths (or shorter the lengths) of the last two dipoles according to certain rules, for both C- and S-chicanes. Such weakening (shortening) becomes more pronounced as the compression factor increases. Note that the above features coincide with the asymmetric DBA-based bunch compressor introduced in [36], where the last dipole is $C^{-1/3}$ or $C^{-1/2}$ times weaker than the 1st dipole. An intriguing pattern emerges that the asymmetric C- and S-chicane, as well as the DBA-based bunch compressor, share similarities and delicately suppress the CSR-induced emittances growth during the compression process.

While the primary focus of this paper lies in analyzing the design principles that effectively suppress CSR-induced emittance growth in the chicane bunch compressors, we also assess the potential microbunching instability associated with the lattice and the beam parameters. Using our developed semi-analytical Vlasov solver [16, 19] enables the fast, efficient evaluation of the various lattice designs. The semi-analytical calculations indicate that these chicane designs, which are ef-

fective in suppressing CSR-induced emittance growth, also exhibit a well-controlled MBI. Specifically, based on the beam parameters and chicane settings presented in Tables I, II, III, and IV, taking into account both the steady-state and transient CSR and the longitudinal space charge effects, the simulation results for the asymmetric C-chicane reveal a maximum gain of about 3.5 occurring around an initial modulation wavelength of $50 \mu\text{m}$. In the case of the asymmetric S-chicane, simulation results demonstrate a maximum gain of 4 around a similar modulation wavelength of $50 \mu\text{m}$. It is worth mentioning that this paper does not consider other collective effects, such as space-charge forces, linac geometric wake field, and many others. For a physically realistic scenario, these are difficult to cancel out and need to be fully taken into account.

We hope that our results can be used as a starting point for practical design, construction and experimental studies on the CSR-immune four-bend chicane compressors. A feasible verification scheme based on the current symmetric C-chicane is, to insert a “negative drift” section between the 2nd and 3rd dipoles, and to increase the strength of the first two dipoles and decrease the last two, while adjusting the longitudinal position of the 2nd and 3rd dipoles by unity. On the other hand, the confirmation of the asymmetric S-chicane design is easily achievable. Based on a symmetric S-chicane, move the position of the 3rd dipole and vary the current of the dipoles to control their bending strength. In addition, asymmetric S-chicane design is also available based on the currently widely used C-chicanes. To obtain the asymmetric S geometries, changing the positive and negative poles of the last two dipole currents seems to be a convenient approach. This paper opens up new avenues for the realisation of CSR-immune bunch compressor, and provide a good guidance for accelerator scientists to respond to the future development of chicane bunch compressor.

ACKNOWLEDGMENTS

This work was supported by the National Natural Science Foundation of China (No. 12275284 and No. 12275094), and the Fundamental Research Funds for the Central Universities (HUST) under Project No. 2021GCRC006. We thank Cai Meng and Wei Li of IHEP for useful discussions.

A. k_i FOR DIFFERENT DIPOLES

Here we assume that the bunch length is constant in a single dipole for point-kick model, so each magnet corresponds to a constant k_i . Concretely, the k_1 for the 1st dipole is $k_1 = k_0 = 0.2459 \frac{N_b r_e}{\gamma \sigma_{z0}^{4/3}}$, reflecting the bunch length at the chicane entrance; the k_2 and k_3 for the 2nd and 3rd dipoles reflect the bunch lengths when crossing the middle position of the dipoles; and the last k_4 reflects the bunch length at the chicane exit.

The value of k_2 for the 2nd dipole is related to k_0 as

$$k_2 = k_0 \frac{\sigma_{z2}^{-4/3}}{\sigma_{z0}^{-4/3}} = \frac{k_0}{(1 + h R_{56}^{s_0 \rightarrow 2m})^{4/3}}, \quad (28)$$

because the bunch length $\sigma_z \approx \sigma_{z0}(1 + h R_{56}^{s_0 \rightarrow s})$ with

$$h = \frac{1 - C}{C R_{56}^{s_0 \rightarrow s_f}}, \quad R_{56}^{s_0 \rightarrow s_f} = -L_{d1} \theta_1^2 (1 + \ell_3 q_3^2), \quad (29)$$

here $C = \sigma_{z0}/\sigma_{zf}$ is the bunch compression factor, h is the linear chirp related to RF cavity phase, $R_{56}^{s_0 \rightarrow s}$ is the first-order longitudinal momentum compaction at location s and the notation “ $s_0 \rightarrow 2m$ ” in $R_{56}^{s_0 \rightarrow 2m}$ means transport from the chicane entrance to the midpoint of the second magnet, which can be written as

$$R_{56}^{s_0 \rightarrow 2m} = -\frac{\theta_1^2}{2} L_{d1}. \quad (30)$$

The value of k_3 for the 3rd dipole is similar to the expression of k_2 as

$$k_3 = k_0 \frac{\sigma_{z3}^{-4/3}}{\sigma_{z0}^{-4/3}} = \frac{k_0}{(1 + h R_{56}^{s_0 \rightarrow 3m})^{4/3}}, \quad (31)$$

with

$$R_{56}^{s_0 \rightarrow 3m} = -L_{d1} \theta_1^2 (1 + \frac{1}{2} \ell_3 q_3^2). \quad (32)$$

The last k_4 reflects the bunch length at the chicane exit (denoted by subscript “ s_f ”) as

$$k_4 = k_0 \frac{\sigma_{z4}^{-4/3}}{\sigma_{z0}^{-4/3}} = C^{4/3} k_0. \quad (33)$$

Equations (19), (20), (22) are the result that applying the k_i under the assumption that the length of L_B is much smaller than L_d .

For S-chicane, the k_1 and k_4 have the same expression as the C-chicane. And the difference is reflected by k_2 and k_3 as

$$k_2 = k_0 \frac{\sigma_{z2}^{-4/3}}{\sigma_{z0}^{-4/3}} = \frac{k_0}{(1 + h R_{56}^{s_0 \rightarrow 2m})^{4/3}}, \quad (34)$$

with

$$h = \frac{1 - C}{C R_{56}^{s_0 \rightarrow s_f}}, \quad R_{56}^{s_0 \rightarrow s_f} = \theta_1^2 L_{d1} (q_2 + q_3 + \ell_2 (1 + q_2) q_3),$$

$$R_{56}^{s_0 \rightarrow 2m} = \frac{L_{d1} \theta_1^2 q_2}{2}. \quad (35)$$

The value of k_3 for the 3rd dipole can be written as

$$k_3 = k_0 \frac{\sigma_{z3}^{-4/3}}{\sigma_{z0}^{-4/3}} = \frac{k_0}{(1 + h R_{56}^{s_0 \rightarrow 3m})^{4/3}}, \quad (36)$$

with

$$R_{56}^{s_0 \rightarrow 3m} = \frac{1}{2} L_{d1} \theta_1^2 (\ell_2 (1 + q_2) q_3 + (2q_2 + q_3)). \quad (37)$$

According to the above calculations, it is not hard to find that the change of bunch length in chicane during the compression process mainly occurs in the 2nd and 3rd dipoles, regardless of C- or S-chicane.

B. THE RESULTS CONSIDERING THE DIPOLE LENGTHS

For asymmetric C-chicane:

After considering the dipole lengths, the drift length between the last two dipoles can be obtain according to Eq. (4) as

$$\ell_3 = -\frac{1}{q_3} - \frac{L_{B1}}{q_3 L_{d1}} - \frac{L_{B3}}{L_{d1}}. \quad (38)$$

The $R_{56}^{s_0 \rightarrow s_f}$, and L_{tot} can be written as

$$L_{tot} = L_{d1} (1 - \frac{1}{q_3}) - L_{B1} (\frac{1}{q_3} - 2) + L_{B3} + L_{d2}^{real}, \quad (39)$$

$$R_{56}^{s_0 \rightarrow s_f} = -\frac{\theta_1^2}{3} (3L_{d1} (1 - q_3) + L_{B1} (2 - 3q_3) - q_3^2 L_{B3}).$$

Here we approximate that the total length are the sum of L_{d1} , L_{nd} , L_{d3} and four dipole lengths. Thus L_{d1} and θ_1 can be expressed as

$$L_{d1} = \frac{q_3 (L_{tot} - L_{d2}^{real} - L_{B1} - L_{B3})}{-1 + q_3} - L_{B1}, \quad (40)$$

$$\theta_1 = \sqrt{\frac{-3R_{56}^{s_0 \rightarrow s_f}}{3(1 - q_3)L_{d1} + (2 - 3q_3)L_{B1} - q_3^2 L_{B3}}}.$$

For asymmetric S-chicane:

After considering the dipole lengths, the variables $\ell_2 = L_{d2}/L_{d1}$, $\ell_3 = L_{d3}/L_{d1}$ can give new expressions as

$$\ell_2 = \frac{4}{q_3} + 3(\frac{q_2}{q_3} + 1) + \frac{L_{B1}}{2L_{d1}q_3} (7 + 6q_2 + 6q_3)$$

$$+ \frac{L_{B2}}{2L_{d1}q_3} (4 + 3q_2 + 2q_3) - \frac{L_{B3}}{2L_{d1}} - \frac{L_{B4}}{2L_{d1}q_3} (1 + q_2 + q_3),$$

$$\ell_3 = -\frac{4}{q_3} - \frac{3q_2}{q_3} - \frac{L_{B1}}{2L_{d1}q_3} (7 + 6q_2) - \frac{L_{B2}}{2L_{d1}q_3} (4 + 3q_2)$$

$$- \frac{L_{B3}}{2L_{d1}} + \frac{L_{B4}}{2L_{d1}q_3} (1 + q_2 + q_3). \quad (41)$$

Here the added condition $L_{d1}/L_{tot} = 1/4$ is rewritten as $(L_{B1} + 0.5L_{B2} + L_{d1})/L_{tot} = 1/4$ in order to fix the position of the 2nd dipole when the total chicane lengths are constant. Equation (24) is tenable if the ℓ_2, ℓ_3 in Eq. (41) are degenerated by setting $L_{Bi} = 0$. One can obtain L_{d1} and the bending angle θ_1

from the value of $R_{56}^{s_0 \rightarrow s_f}$, L_{tot} according to

$$\begin{aligned} L_{tot} &= 4(L_{B1} + 0.5L_{B2} + L_{d1}) = 4L_{B1} + 2L_{B2} + 4L_{d1}, \\ R_{56}^{s_0 \rightarrow s_f} &= \theta_1^2 \left((L_{d1}q_2 + L_{d3}q_3q_4) + \frac{L_{B1}}{6}(1 + 3q_2) + \frac{L_{B2}}{6}q_2(3 + q_2) \right) \\ &\quad + \frac{\theta_1^2 L_{B4}}{6}(1 + 2q_2 + q_2^2 - q_3 - q_2q_3 - 2q_3^2) \\ &\quad - \frac{\theta_1^2 L_{B3}}{6}q_3(3 + 3q_2 + 2q_3). \end{aligned} \quad (42)$$

C. DERIVATION OF THE ENTRIES OF R-MATRIX

Considering the variation of bunch length within each dipole, the bunch parameters k_1, k_2, k_3, k_4 in Eq. (13) are no longer set to a fixed value for each dipole, but are modified as follows

$$k_i = \frac{k_0}{(1 + h R_{56}^{s_0 \rightarrow s})^{4/3}}, \quad (i = 1, 2, 3, 4) \quad (43)$$

where $R_{56}^{s_0 \rightarrow s}$ in different positions, as a function of ϕ , are expressed in Appendix C. Here ϕ and the subscript “s” are the angle and position that the beam traverses in a dipole magnet, respectively. Thus the CSR cancelation conditions for a chicane can be evaluated using an integration method as [38]

$$\begin{aligned} \Delta x_f^2 &= \left[\sum_{i=1}^4 \rho_i^{1/3} \int_B k_i R_{16}^{s \rightarrow s_f} d\phi \right]^2 = 0, \\ \Delta x_f'^2 &= \left[\sum_{i=1}^4 \rho_i^{1/3} \int_B k_i R_{26}^{s \rightarrow s_f} d\phi \right]^2 = 0, \end{aligned} \quad (44)$$

here both $R_{16}^{s \rightarrow s_f}$ and $R_{26}^{s \rightarrow s_f}$ vary as a function of ϕ in dipoles.

For asymmetric C-chicane:

For s within the 1st bend:

$$\begin{aligned} R_{16}^{s \rightarrow s_f} &= L_{d1}(\theta_1 - \theta_{1s}) - (2L_{B3} + L_{d3} + L_{d2})\theta_{1s} \\ &\quad + L_{B1}(\theta_1 - 2\theta_{1s} + \frac{\theta_{1s}^2}{2\theta_1}) + (L_{B2} + L_{d3})\theta_3, \\ R_{26}^{s \rightarrow s_f} &= -\theta_{1s}, \\ R_{56}^{s_0 \rightarrow s} &= \frac{L_{B1}\theta_{1s}^3}{6\theta_1}, \end{aligned} \quad (45)$$

with $\theta_{1s} = \theta_1 s / L_{B1}$, and $0 \leq s \leq L_{B1}$.

For s within the 2nd bend:

$$\begin{aligned} R_{16}^{s \rightarrow s_f} &= -(\theta_1 + \theta_{2s})(2L_{B3} + L_{d3} + L_{d2}) - \frac{L_{B1}(\theta_1 + \theta_{2s})^2}{2\theta_1} \\ &\quad + (L_{B2} + L_{d3})\theta_3, \\ R_{26}^{s \rightarrow s_f} &= -(\theta_1 + \theta_{2s}), \\ R_{56}^{s_0 \rightarrow s} &= L_{d1}\theta_1\theta_{2s} + \frac{L_{B1}}{6} \left(\theta_1^2 + 3\theta_1\theta_{2s} - 3\theta_{2s}^2 - \frac{\theta_{2s}^3}{\theta_1} \right), \end{aligned} \quad (46)$$

with $\theta_{2s} = -\theta_1 s / L_{B1}$, and $0 \leq s \leq L_{B1}$.

For s within the 3rd bend:

$$\begin{aligned} R_{16}^{s \rightarrow s_f} &= L_{d3}(\theta_3 - \theta_{3s}) + L_{B3} \left(\theta_3 - 2\theta_{3s} + \frac{\theta_{3s}^2}{2\theta_3} \right), \\ R_{26}^{s \rightarrow s_f} &= -\theta_{3s}, \\ R_{56}^{s_0 \rightarrow s} &= \frac{L_{B3}\theta_{3s}^3}{6\theta_3} + L_{d1}\theta_1(-\theta_1 + \theta_{3s}) + L_{B1} \left(-\frac{2\theta_1^2}{3} + \theta_1\theta_{3s} \right), \end{aligned} \quad (47)$$

with $\theta_{3s} = \theta_3 s / L_{B3}$, and $0 \leq s \leq L_{B3}$.

For s within the last bend:

$$\begin{aligned} R_{16}^{s \rightarrow s_f} &= -\frac{L_{B3}(\theta_3 + \theta_{4s})^2}{2\theta_3}, \\ R_{26}^{s \rightarrow s_f} &= -\theta_3 - \theta_{4s}, \\ R_{56}^{s_0 \rightarrow s} &= L_{d1}\theta_1(-\theta_1 + \theta_3 + \theta_{4s}) + L_{d3}\theta_3\theta_{4s} \\ &\quad + \frac{L_{B1}\theta_1}{3}(-2\theta_1 + 3\theta_3 + 3\theta_{4s}) + \frac{L_{B3}}{6}(\theta_3^2 + 3\theta_3\theta_{4s} - 3\theta_{4s}^2 - \frac{\theta_{4s}^3}{\theta_3}), \end{aligned} \quad (48)$$

with $\theta_{4s} = -\theta_3 s / L_{B4}$, and $0 \leq s \leq L_{B4}$.

For asymmetric S-chicane:

For s within the 1st bend:

$$\begin{aligned} R_{16}^{s \rightarrow s_f} &= \frac{\theta_{1s}}{2(\theta_1 + \theta_2)} (-L_{B2} + 2L_{d1})\theta_2 + (L_{B3} + 2L_{d3})\theta_3 \\ &\quad + \frac{L_{B1}\theta_{1s}}{2\theta_1(\theta_1 + \theta_2)} (-\theta_1^2 + \theta_1(\theta_{1s} - 2\theta_2) + \theta_{1s}\theta_2) \\ &\quad - \frac{\theta_{1s}}{2(\theta_1 + \theta_2)} L_{B4}(2\theta_1 + \theta_4), \\ R_{26}^{s \rightarrow s_f} &= -\theta_{1s}, \\ R_{56}^{s_0 \rightarrow s} &= \frac{L_{B1}\theta_{1s}^3}{6\theta_1}, \end{aligned} \quad (49)$$

with $\theta_{1s} = \theta_1 s / L_{B1}$, and $0 \leq s \leq L_{B1}$.

For s within the 2nd bend:

$$\begin{aligned} R_{16}^{s \rightarrow s_f} &= \frac{1}{2} (2(L_{B3} + L_{B4} + L_{d2} + L_{d3})(\theta_2 - \theta_{2s})) \\ &\quad + \frac{1}{2} \left(L_{B3}\theta_3 + 2(L_{B4} + L_{d3})\theta_3 + L_{B4}\theta_4 + \frac{L_{B2}(\theta_2 - \theta_{2s})^2}{\theta_2} \right), \\ R_{26}^{s \rightarrow s_f} &= -\theta_1 - \theta_{2s}, \\ R_{56}^{s_0 \rightarrow s} &= L_{d1}\theta_1\theta_{2s} + \frac{L_{B1}}{6} (\theta_1^2 + 3\theta_1\theta_{2s}) + \frac{\theta_{2s}^2 L_{B2}(3\theta_1 + \theta_{2s})}{6\theta_2}, \end{aligned} \quad (50)$$

with $\theta_{2s} = \theta_2 s / L_{B2}$, and $0 \leq s \leq L_{B2}$.

For s within the 3rd bend:

$$\begin{aligned}
R_{16}^{s \rightarrow s_f} &= \frac{1}{2} \left(2(L_{B4} + L_{d3})(\theta_3 - \theta_{3s}) + \frac{L_{B3}(\theta_3 - \theta_{3s})^2}{\theta_3} + L_{B4}\theta_4 \right), \\
R_{26}^{s \rightarrow s_f} &= \theta_3 + \theta_4 - \theta_{3s}, \\
R_{56}^{s_0 \rightarrow s} &= \frac{1}{6} (L_{B1}\theta_1^2 + L_{B2}\theta_2^2 + 3\theta_1\theta_2(L_{B1} + L_{B2} + 2L_{d1})) \\
&\quad - \frac{\theta_{3s}}{2} (-\theta_4(L_{B4} + 2L_{d3}) + L_{B3}(2\theta_1 + 2\theta_2 + \theta_3)) \\
&\quad + \frac{L_{B3}\theta_{3s}^2}{6\theta_3} (3\theta_1 + 3\theta_2 + \theta_{3s}),
\end{aligned} \tag{51}$$

with $\theta_{3s} = \theta_3 s / L_{B3}$, and $0 \leq s \leq L_{B3}$.

For s within the last bend:

$$\begin{aligned}
R_{16}^{s \rightarrow s_f} &= \frac{L_{B4}(\theta_4 - \theta_{4s})^2}{2\theta_4}, \\
R_{26}^{s \rightarrow s_f} &= \theta_4 - \theta_{4s}, \\
R_{56}^{s_0 \rightarrow s} &= -\frac{\theta_3}{6} (3L_{B3}(\theta_1 + \theta_2) + 2L_{B3}\theta_3 - 6(L_{B4} + L_{d3})\theta_4 + 3L_{B4}\theta_4) \\
&\quad + \frac{1}{6} (6L_{d1}\theta_1\theta_2 + L_{B2}\theta_2(3\theta_1 + \theta_2) + L_{B1}\theta_1(\theta_1 + 3\theta_2)) \\
&\quad + \frac{1}{6} (3L_{B4}\theta_4\theta_{4s} - 3L_{B4}\theta_4\theta_{4s}^2) + \frac{1}{6\theta_4} L_{B4}\theta_{4s}^3,
\end{aligned} \tag{52}$$

with $\theta_{4s} = \theta_4 s / L_{B4}$, and $0 \leq s \leq L_{B4}$.

-
- [1] International Linear Collider, Technical Design Report, 2013, <http://www.linearcollider.org/ILC/Publications/Technical-Design-Report>.
- [2] Bentson, L & Emma, P. & Krejcik, Patrick. "A New Bunch Compressor Chicane for the SLAC Linac to Produce 30-fsec, 30-kA, 30-GeV Electron Bunches," NASA STI/Recon Technical Report N. 10.2172/799087 (2002).
- [3] E. Esarey, C. B. Schroeder and W. P. Leemans, *Rev. Mod. Phys.* **81**, 1229-1285 (2009).
- [4] C. A. Lindström, "Staging of plasma-wakefield accelerators," *Phys. Rev. Accel. Beams* **24**, 014801 (2021).
- [5] M. Borland, "Design and performance simulations of the bunch compressor for the Advanced Photon Source low-energy undulator test line free electron laser," *Phys. Rev. ST Accel. Beams* **4**, 074201 (2001).
- [6] Kang, H. S. et al. "FEL performance achieved at PAL-XFEL using a three-chicane bunch compression scheme," *J. of synchrotron rad.*, 26(4), 1127-1138 (2019).
- [7] T. Tanaka and T. Shintake, Spring-8 compact SASE source conceptual design report, Technical Report, 2005.
- [8] R. Ganter, Swiss FEL-conceptual design report, Paul Scherrer Institute (PSI) Technical Report No. PSI-10-04, 2010.
- [9] J. Arthur, P. Anfinrud, and P. Audebert, LCLS conceptual design report, SLAC Technical Report No. SLAC-R-593, 2002.
- [10] Stulle, Frank. "A bunch compressor for small emittances and high peak currents at the VUV Free-Electron Laser," (2004). DOI:10.3204/DESY-THESIS-2004-041
- [11] Y. S. Derbenev, J. Rossbach, E. L. Saldin and V. D. Shiltsev, "Microbunch radiative tail - head interaction," PRINT-98-023, TESLA-FEL-95-05 (1995). doi:10.3204/PUBDB-2018-04128
- [12] E. L. Saldin, E. A. Schneidmiller and M. V. Yurkov, "On the coherent radiation of an electron bunch moving in an arc of a circle," *Nucl. Instrum. Meth. A* **398**, 373-394 (1997).
- [13] M. Dohlus and T. Limberg, "Emittance growth due to wake fields on curved bunch trajectories," *Nucl. Instrum. Meth. A* **393**, 490-493 (1997) DESY-TESLA-FEL-96-13G.
- [14] H. H. Braun, R. Corsini, L. Groening, F. Zhou, A. Kabel, T. O. Raubenheimer, R. Li and T. Limberg, *Phys. Rev. ST Accel. Beams* **3**, 124402 (2000).
- [15] S. Heifets, G. Stupakov and S. Krinsky, "Coherent synchrotron radiation instability in a bunch compressor," *Phys. Rev. ST Accel. Beams* **5**, 064401 (2002).
- [16] C. Y. Tsai, W. Qin, K. Fan, X. Wang, J. Wu and G. Zhou, "Theoretical formulation of phase space microbunching instability in the presence of intrabeam scattering for single-pass or recirculation accelerators," *Phys. Rev. Accel. Beams* **23**, 124401 (2020).
- [17] C. Y. Tsai, Y. S. Derbenev, D. Douglas, R. Li and C. Tennant, "Vlasov analysis of microbunching instability for magnetized beams," *Phys. Rev. Accel. Beams* **20**, 054401 (2017).
- [18] E. Roussel, E. Ferrari, E. Allaria, G. Penco, S. Di Mitri, M. Veronese, M. Danailov, D. Gauthier and L. Giannessi, "Multicolor High-Gain Free-Electron Laser Driven by Seeded Microbunching Instability," *Phys. Rev. Lett.* **115**, 214801 (2015).
- [19] C. Y. Tsai, S. Di Mitri, D. Douglas, R. Li and C. Tennant, "Conditions for coherent-synchrotron-radiation-induced microbunching suppression in multibend beam transport or recirculation arcs," *Phys. Rev. Accel. Beams* **20**, 024401 (2017).
- [20] Z. Huang and K. Kim, "Formulas for coherent synchrotron radiation microbunching in a bunch compressor chicane," *Phys. Rev. ST Accel. Beams* **5**, 074401 (2002).
- [21] M. Venturini, "Microbunching instability in single-pass systems using a direct two-dimensional Vlasov solver," *Phys. Rev. ST Accel. Beams* **10**, 104401 (2007).
- [22] M. Venturini, R. Warnock and A. Zholents, "Vlasov solver for longitudinal dynamics in beam delivery systems for x-ray free electron lasers," *Phys. Rev. ST Accel. Beams* **10**, 054403 (2007).
- [23] C. Y. Tsai, "Concatenated analyses of phase space microbunching in high brightness electron beam transport," *Nucl. Instrum. Methods Phys. Res., Sect. A*, (2019). doi:10.1016/J.NIMA.2019.06.061
- [24] F. Stulle, A. Adelman and M. Pedrozzi, "Designing a bunch compressor chicane for a multi-TeV linear collider," *Phys. Rev. ST Accel. Beams* **10**, 031001 (2007).
- [25] C. Mitchell, J. Qiang and P. Emma, *Phys. Rev. ST Accel. Beams* **16**, 060703 (2013).
- [26] G. Penco, M. Danailov, A. Demidovich, E. Allaria, G. De Nino, S. Di Mitri, W. M. Fawley, E. Ferrari, L. Giannessi and M. Trovó, *Phys. Rev. Lett.* **112**, 044801 (2014).
- [27] D. Xiang and A. Chao, *Phys. Rev. ST Accel. Beams* **14**, 114001 (2011).
- [28] M. Cornacchia and P. Emma, *Phys. Rev. ST Accel. Beams* **5**, 084001 (2002).

- [29] Yakimenko, Vitaly et al. “Experimental observation of suppression of coherent-synchrotron-radiation-induced beam-energy spread with shielding plates,” *Phys. Rev. Lett.* **16**, 060703 (2013).
- [30] D. Douglas, “Suppression and enhancement of CSR-driven emittance degradation in the IR-FEL driver,” Thomas Jefferson National Accelerator Facility Report, Technical Report No. JLAB-TN-98-012, 1998.
- [31] R Hajima, “Emittance compensation in a return arc of an energy-recovery linac,” *Nucl. Instrum. Methods Phys. Res., Sect. A*, **528**, 335-339, (2004).
- [32] Y. Jiao, X. Cui, X. Huang and G. Xu, “Generic conditions for suppressing the coherent synchrotron radiation induced emittance growth in a two-dipoles achromat,” *Phys. Rev. ST Accel. Beams* **17**, 060701 (2014).
- [33] X. Y. Huang, Y. Jiao, X. H. Cui and G. Xu, *Chin. Phys. C* **39** (2015) 057001.
- [34] S. Di Mitri, M. Cornacchia and S. Spampinati, “Cancellation of coherent Synchrotron Radiation kicks with optics balance,” *Phys. Rev. Lett.* **110**, 014801 (2013).
- [35] S. Di Mitri and M. Cornacchia, “Transverse emittance-preserving arc compressor for high-brightness electron beam-based light sources and colliders,” *EPL* **109**, 62002 (2015).
- [36] C. Zhang, Y. Jiao, W. Liu and C. Y. Tsai, “Suppression of the coherent synchrotron radiation induced emittance growth in a double-bend achromat with bunch compression,” *Phys. Rev. Accel. Beams* **26**, 050701 (2023).
- [37] S. Di Mitri, “Feasibility study of a periodic arc compressor in the presence of coherent synchrotron radiation,” *Nucl. Instrum. Meth. A* **806**, 184-192 (2016).
- [38] P. Emma and R. Brinkmann, “Emittance dilution through coherent energy spread generation in bending systems,” *Conf. Proc. C 970512*, 1679 (1997) SLAC-PUB-7554.
- [39] M. Venturini, “Design of a triple-bend isochronous achromat with minimum coherent-synchrotron-radiation-induced emittance growth,” *Phys. Rev. Accel. Beams* **19**, 064401 (2016).
- [40] Hajima, Ryoichi, “A First-Order Matrix Approach to the Analysis of Electron Beam Emittance Growth Caused by Coherent Synchrotron Radiation,” *Jap. J. Appl. Phys.* **42**, L974 (2003).
- [41] Y. Jing, Y. Hao and V. N. Litvinenko, “Compensating effect of the coherent synchrotron radiation in bunch compressors,” *Phys. Rev. ST Accel. Beams* **16**, 060704 (2013).
- [42] D. Z. Khan and T. O. Raubenheimer, “Novel bunch compressor chicane: The five-bend chicane,” *Phys. Rev. Accel. Beams* **25**, 090701 (2022).
- [43] Beutner, Bolko. “Measurement and analysis of coherent synchrotron radiation effects at FLASH.” (2007).
- [44] S. A. Antipov, A. F. Pousa, I. Agapov, R. Brinkmann, A. R. Maier, S. Jalas, L. Jeppe, M. Kirchen, W. P. Leemans and A. M. de la Ossa, *et al.* “Design of a prototype laser-plasma injector for an electron synchrotron,” *Phys. Rev. Accel. Beams* **24**, 111301 (2021).
- [45] Chao, A. W., *Lectures on accelerator physics* (World Scientific, 2020), p. 127.
- [46] B. Beutner, “Measurement and Analysis of Coherent Synchrotron Radiation Effects at FLASH,” doi:10.3204/DESY-THESIS-2007-040.
- [47] M. Borland, “elegant: A Flexible SDDS-Compliant Code for Accelerator Simulation,” Argonne National Lab., IL, Technical Report No. LS-287, (2000).
- [48] M. Borland, “Simple method for particle tracking with coherent synchrotron radiation,” *Phys. Rev. ST Accel. Beams* **4**, 070701 (2001).